NASA Technical Memorandum 107361

Numerical Flow Visualization in Basic- and Hyper-Cluster Spheres

R.C. Hendricks
Lewis Research Center
Cleveland, Ohio

M.M. Athavale
CFD Research Corporation
Huntsville, Alabama

M.J. Braun
University of Akron
Akron, Ohio

S. Lattime
B&C Engineering
Akron, Ohio

Prepared for the
First Pacific Symposium on Flow Visualization and Image Processing
sponsored by the Pacific Center of Thermal-Fluids Engineering
Honolulu, Hawaii, February 23–26, 1997

National Aeronautics and
Space Administration

NUMERICAL FLOW VISUALIZATION IN BASIC- AND HYPER-CLUSTER SPHERES

R.C. Hendricks
NASA Lewis Research Center
Cleveland, Ohio 44135, USA

M. M. Athavale
CFD Research Corporation
Huntsville Alabama 35805

M.J. Braun
University Of Akron
Akron Ohio 44325

S. Lattime
B&C Engineering
Akron Ohio 44325

ABSTRACT

Packed spherical particle beds have wide applications throughout the process industry and are usually analyzed using an appropriate combination of laminar and turbulent flows with empirically derived coefficients of which the Ergun (1952) relation is probably the best known. The 3-D complexity of the void distribution within the beds has precluded detailed studies of sphere clusters. Numerical modeling and flow vector visualization for the basic tetra- and hexa-sphere clusters and two hyper-sphere clusters are presented at two Reynolds numbers, 400 and 1200. Cutting planes are used to enable visualization of the complex flows generated within the sphere clusters and are discussed herein. The boundary conditions and flow fields for the simple clusters are also compared to the hyper-clusters with larger variations found for hexa-clusters.

INTRODUCTION

Although flow in packed beds of spheres may be correlated in the same manner as flows through brush seals and arrays of pins (cylinders) via the simple combination of laminar and turbulent flows with appropriate coefficients (e.g., Bird et al. (1960), Hendricks et al. (1996)) yet flow details have not been delineated. The complexity of any useful bed of spheres includes occlusions, voids, irregular and different diameter spheres, compaction strains, crushed and cracked spheres, debris holdup and variations in thermophysical properties. At this point, these factors will be considered secondary in an attempt to calculate and visualize the flow in a regular bed. More details on flows in regular beds of spheres can be found in Athavale et al. (1994a).

Visualization of flows in packed beds of spheres as described herein is comprised of (1) mathematical modeling and numerical representation of the flow fields and (2) physical modeling and laser sheet illumination of flow field particles. Unlike visualization of flows in pinned arrays and brush seals which are weakly 3-D dependent, flow, heat and mass transfer in spherical beds are strongly 3-D dependent and require the combined efforts of numerical and experimental techniques to embody and characterize models and results.

BASIC SPHERICAL CLUSTERS

Hexagonal or cubic densely packed beds have 12 neighbors and a void fraction of about 0.26, Fig. 1. Two basic spaces can be identified:

Tetra-space.—The unit is formed of four (4) spheres with centers at the apex of a tetrahedron. Three spheres lie in a plane touching one another with the centers forming an equilateral triangle. The fourth sphere is placed in the hollow formed by the three spheres forming a regular tetrahedron. Thus there are four (4) open curvilinear triangular faces for flow and four (4) spherical triangular surfaces or boundaries, Fig. 2(a). Alternately, a half tetra-space unit is the three spheres in a plane with a sphere placed in the hollow on each side and the plane of symmetry passing through the centers forming an equilateral triangle.

Hexa-space.—The unit is formed from six (6) spheres. Three spheres lie in one plane touching one another with centers forming a equilateral triangle and three others lie in a second plane stacked upon the first plane and rotated 60° to fit the hollow of those in the first plane emulating a six pointed star. An alternate method of constructing this space is to arrange four spheres in a plane at corners of a square, and place two spheres in the hollows of the layer one on each side. The centers of the spheres form a double pyramid. To visualize this, rotate the hexa-space, figure 1, about the solid horizontal line (upper layer-2), away from the viewer, until the solid and dashed horizontal line (lower layer-1) coincide. In this view the double pyramidal structure becomes apparant. This space has eight (8) open faces for flow and six (6) spherical rectangular surfaces or boundaries, Fig. 2(b).

Subdomains of the tetra and hexa Interstitial Spaces

To generate subdomains that can be repeated, a common shared point(centroid) edges and surfaces are required. The centroid of interstitial space was taken as this point, with straight lines between the centroid and the corners of the open faces defining the shared edges and shapes of the subdomains. These subdomains are either tetrahedral or pyramidal in shape, and are defined either with the open area or the curved surfaces of the sphere as the basis that is joined to the apex located at the central point.

Tetrahedral-1.—This subdomain has the triangular curved sphere surface as the base Fig. 3(a). The base shape is generated in tetra-space. The corners of the triangle are joined to the apex to form the subdomain and is needed only for tetra-spaces.

Tetrahedral-2.—This subdomain has the flat, open area shown in Fig. 3(b) as the base, and the three corners are joined to the central apex to form the subdomain (Fig. 3(c)). Since the subdomain has the open cutting plane as the base it is required in both tetra- and hexa-spaces when forming hyperclusters.

Pyramidal.—This subdomain has a quadrilateral portion of the sphere surface as the base, and the four corners are joined to the apex to form the subdomain, Fig. 3(d) and required only in the hexa-space.

A compilation of the subdomains and the corresponding surface grids are shown in Figs. 3(e) to 3(g). The axis convention for grid generation are illustrated in Fig. 4(a) for tetrahedral-1, Fig. 4(b) for tetrahedral-2 and Fig. 4(c) for pyramidal.

The geometries of the spaces are complex, and a global axis convention as well as numbering sphere locations was found to be necessary and convenient in describing the geometry as well as analyzing the flow-field. This convention is shown in Figs. 5(a) and (b).

The interstitial spaces are created using a group of the subdomain with the apexes coincident at the space centroid. Tetrahedral domains are used for all open faces and walls in the tetra-space with pyramidal domains used for walls in the hexa-space. All apexes coincide at the center of the interstitial space which implies a polar point. Tetrahedral domains also have a polar line or centerline. Each tetra-space has 8 domains and each hexa-space has 14 domains.

The tetra-space has tetrahedral-1 subdomains on the sphere surfaces and four tetrahedral-2 subdomains on the four open faces, Fig. 6(a). The hexa-space had six surrounding spheres, with bases on the sphere surfaces. Eight cutting planes with eight open area used as bases for the tetrahedral-2 subdomains, Fig. 6(b).

The packed bed is generated by populating a region with the tetra- and hexa-spaces joined at the open faces in each. Care is needed to ensure that the resulting clusters generate the original sphere surfaces correctly. Two types of first-level hyperclusters are possible:

Hypercluster-1.—Tetra-space connected to 3 hexa-spaces and one plane of symmetry with 54 domains, Fig. 7(a).

Hypercluster-2.—Hexa-space connected to 8 tetra-spaces with 78 domains Fig. 7(b).

An algebraic grid generator was used to generate clustered grids in each of the subdomains which were then assembled to form multiblock grids for the interstitial spaces and hyperclusters. The tetra-space had 30(i)x10(j)x10(k) for each domain (24000 cells), while the hexa-space had 8x8x8 pyramid domain, 24(i)x8(j)x8(k) tetrahedral domain (15 360 cells). The clusters had 24x8x8 for the tetrahedral domain and 8x8x8 for the pyramidal domain.

Flow Solver

The numerical simulations were performed using SCISEAL, a pressure based, finite volume 3-D CFD code with implicit multiblock capability, Athavale et al. (1994b). The working fluid was nitrogen gas at pressures of 1.5 MPa. The flow Reynolds numbers were 400 and 1200 and the flow was assumed to be laminar with constant gas properties. The boundary conditions for the single tetra- and hexa-spaces are shown in Figs. 6(a) and (b). Similar conditions were also used for the two hyperclusters.

RESULTS

Tetra-space

Included here are several representative velocity vector plots for two Reynolds numbers 400 and 1200, taken along selected cutting planes. Figure 8(a) shows the velocity vectors at x = 1.1 cutting plane, which is a little to the right of the symmetry plane at x = 1.0, see Fig. 5(a). The uniform, parallel inlet velocity is seen on the left edge of both plots in Fig. 8(a). The frontal stagnation zone created by the incoming flow on sphere 3 is seen on the right side, and the large recirculation region at the bottom of the figure is created by a combination of the stagnation on sphere 3 and the symmetry boundary on the bottom plane of the tetra-space. As expected, this recirculation zone is somewhat stronger in the high Reynolds number flow. In the upper portion, the flow splits and moves upwards (in +z direction) and sideways (± x-directions) as it exits through the open areas on either side of sphere 3. There is evidence of separation of the flow on the upper wall, but the strength of this recirculation zone is nearly the same for both Reynolds numbers.

The incoming flow generates separation bubbles near the surfaces of spheres 1 and 2 (due to the surface curvature); to see these zones, vector plots along the z = 0.18 cutting plane are shown in Fig. 8(b). The largest contrast between the two Reynolds number flows is seen in this figure. A double vortex is seen in the plot for the higher Reynolds number flow, which is nearly absent in the low Reynolds number case. The effect of this bubble would have a direct impact on surface temperature distributions for example. The frontal stagnation zone on the surface of sphere 3 is seen in both the plots.

Vector plots along the y = 0.63 cutting plane are shown in Fig. 8(c) and part of the separation zones on sphere 1 and 2 are seen. The incoming flow is out of the plane of the paper. The flow near the sphere surfaces in both cases turns upwards as it moves toward the exit boundaries on either side of the plots. The recirculation bubbles for the higher Reynolds number flows are again seen to be a little stronger.

Hexa-space

The hexa-space flow is more complex due to multiple inlet boundaries, Fig. 6(b). The velocites at the x = 1.0 cutting plane (a symmetry plane) are shown in Fig. 9(a). The front stagnation region on sphere 3 is seen in both plots and a very weak recirculation in the central portion. A recirculation zone near the open bottom surface is seen, and is nearly the same for both Reynolds numbers. This recirculation is also seen to draw fluid in through the bottom face. Flow near sphere 3 turns upwards as it exits though the open face on the right. A central vortex is seen on the symmetry boundary in both cases, and is a result of the upward flow motion on the right side, which forces the flow to go in the negative z direction under the surface of sphere 4. The incoming flow on either side of sphere 4 produces a double vortex under this sphere, which is seen in the z = 1.04 section, Fig. 9(b). The double vortex is somewhat stronger and smaller in the higher Reynolds number case. This double vortex

forces the flow in the negative y and z directions under sphere 4, and this was also seen in the previous figure. At a lower section z = 0.36, Fig. 9(c), the incoming flow generates symmetric vortices near the surfaces of spheres 1 and 2 as in the case of the tetra-space, and the vortices are stronger for the higher Reynolds number. Vector plots at y = 0.58 cutting plane are shown in Fig. 9(d). The double vortex is seen under sphere 4 in both plots. The flow is out of the plane of the paper. A small recirculation is seen near the top open face which indicates some inflow as well as some outflow in this face. The overall structure of the flow, except the central double vortex is quite similar for the two Reynolds numbers.

Hypercluster -1

The central cutting plane at x = 1.01 Fig. 10(a) shows the incoming flow at the left, which now show some variation in the velocity magnitudes (Reynolds number of 1200), including some evidence of small recirculations near the x-y plane, where a sphere surface from the adjoining hexa-space is present. The recirculation bubble in the central tetra-space near the bottom edge is weaker and smaller in size as a result of the inclination of the incoming flow through the plane on the left. There is also some evidence of recirculation near the top edge, as the flow exits through the right-side boundary.

The vector plot along, z = 0.18 shown in Fig. 10(b) has some differences from the single molecule plot Fig. 8(b). Although the velocity pattern near the spheres 1 and 2 is similar, the hyper-cluster solution shows an absence of the double vortical structure seen in Fig. 8(b.2). The y = 0.63 plane, Fig. 10(c) shows a flow pattern similar to that for the single tetra-space Fig. 8(c.2). Several recirculation zones exist in the region attached to the central interstitial space shown in these figures. The solutions on the single spaces were obtained using a specified constant pressure on the exit boundaries. The pressure values on the corresponding interfaces in the central tetra-space were checked to assess the validity of this assumption. The overall pressure variation across these faces was found to be sufficiently small to justify the constant value assumption used in the single space calculations. Pressure plots were developed but not reported herein.

Hypercluster-2

Six pyramidal subdomains in the central hexa-space and 72 tetrahedral subdomains for a total of 113664 cells. The velocity vectors (Reynolds number of 1200) along the plane at x = 1.0 are shown in Fig. 11(a). As in the previous case some differences from its single-space counterpart Fig. 9(a.2), are noted. The incoming flow from the left edge has a faster portion near the top edge which is a result of the tetra-space present on the left of this interface. This jet tends to destroy the weak central recirculation zone seen earlier. The recirculation zone near the bottom interface is still present, and the double vortical structure under sphere 4 is seen. The plane along z = 1.04 also shows this double vortex clearly in Fig. 11(b.1). However, the vortex is somewhat weakened due to the change in the inlet velocity profiles at the interface boundaries on either side of sphere 4. The section along z = 0.36 in Fig. 11(b.2), however shows a nearly smooth flow along the spheres 1 and 2 while the single space counterpart Figs. 9(b.2) and (c.2) show a vortex near the sphere surfaces. As in the case of hypercluster-1, this is due to the inclination of the incoming flow. The double vortex under sphere 4 is also seen in the y = 0.58 plane shown in Fig. 11(c). This figure also shows the changes that are present in the inlet flows on either side of sphere 4, where the flow exits tetra-spaces attached to the central hexa-space, compare with Fig. 9(d.2).

SUMMARY

Two basic interstitial flow geometries, tetra- and hexa-spaces, have been identified as essential elements for generating hexagonal or cubic densely packed ideal beds. The interstitial spaces were divided into suitable subdomains for structured grid generation and subsequent solutions. The flow solver SCISEAL, a pressure based multidomain Navier-Stokes solver was used to obtain representative flow solutions on the tetra- and hexa-spaces as well as first-level hyperclusters generated using the basic spaces.

The flow is fully 3-D and complex with multiple vortical structures that generate local stagnation, separations, and most importantly flow threads or fast flowing regions in the direction of the bulk flow field.

Preliminary solutions on first level hyperclusters indicate that the results differ from the basic structures; still the major vortical structures and flow threads remained.

The vortical structures and local stagnation zones are inferred to have a significant influence on transport phenomena.

The results, although not compared herein, are in good qualitative agreement with experimental observation.

REFERENCES

Athavale, M.M., Przekwas, A.J., Braun, M.J. (1994a) Flow and Heat Transfer Analysis for Packed Beds on Heated Spheres. Part 1: Numerical Computations. Final Report Contract NAS3–25967. NASA Lewis Research Center, Cleveland Ohio.

Athavale, M.M., Przekwas, A.J., Hendricks, R.C., and Liang, A., (1994b) A SCISEAL: A Three-Dimensional CFD Code for Accurate Analyses of Fluid Flow and Forces in Seals, 1994 Conference on Advanced Earth-to-Orbit Propulsion Technology, NASA Marshall Space Flight Center, May 1994.

Bird, R.B., Stewart, W.E., and Lightfoot, E.N.(1960), Transport Phenomena, John Wiley Press, New York, p. 200.

Ergun, S. (1952) Chem Engr. Prog. 43(92).

Hendricks, R.C., Kudriavtsev, V.V., Braun, M.J., Athavale, M.M. Flows in Pinned Arrays Simulating Brush Seals - to be presented at the Int. Cong. On Fluid Dynamics, Dec. 29-31, 1996 Cairo Egypt.

Kerrebrock, J.L. and Kalamas, J. (1993) Flow Instability in Particle-Bed Nuclear Reactor, AIAA–93–1758.

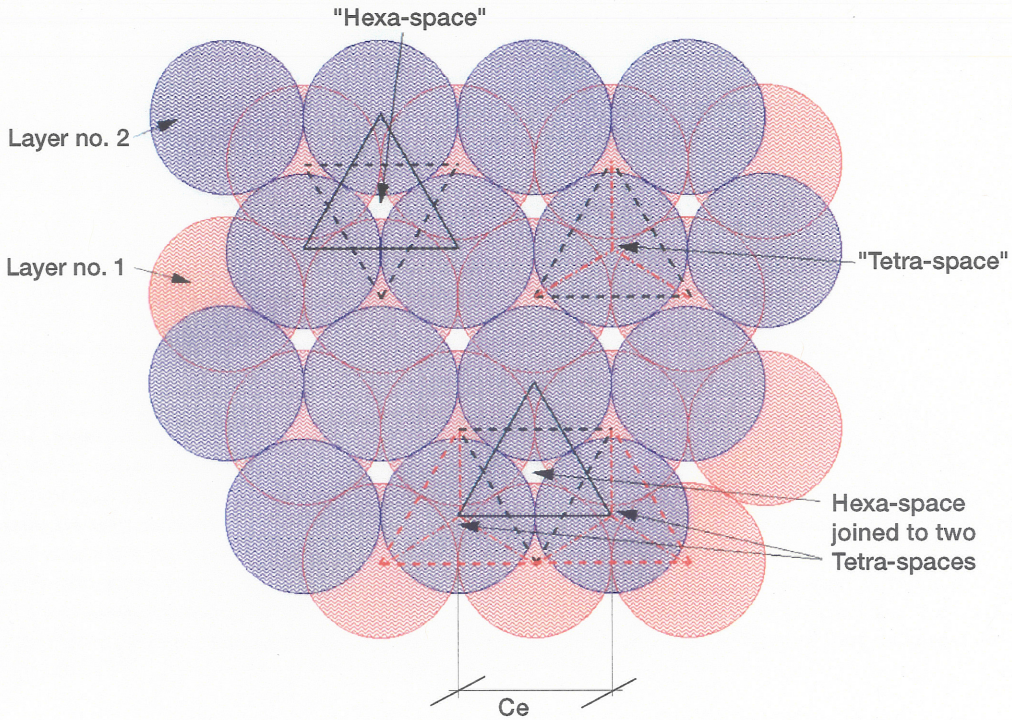

Figure 1.—Stacking of sphere layers to generate densely-packed arrangements.

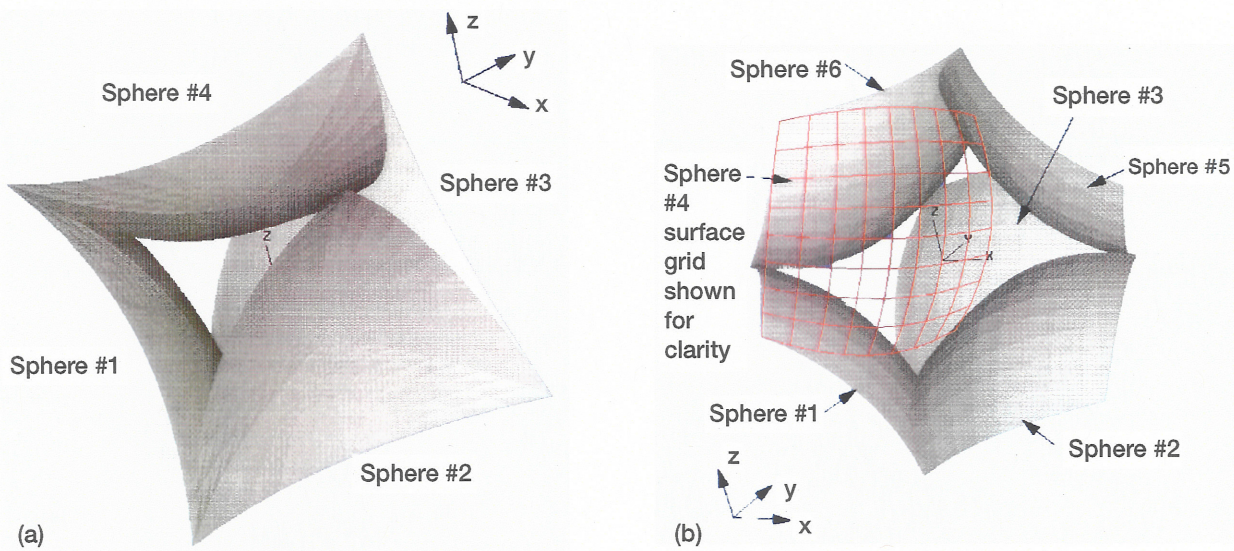

Figure 2.—(a) Solids model for the tetra-space. (b) Solids model for hexa-space.

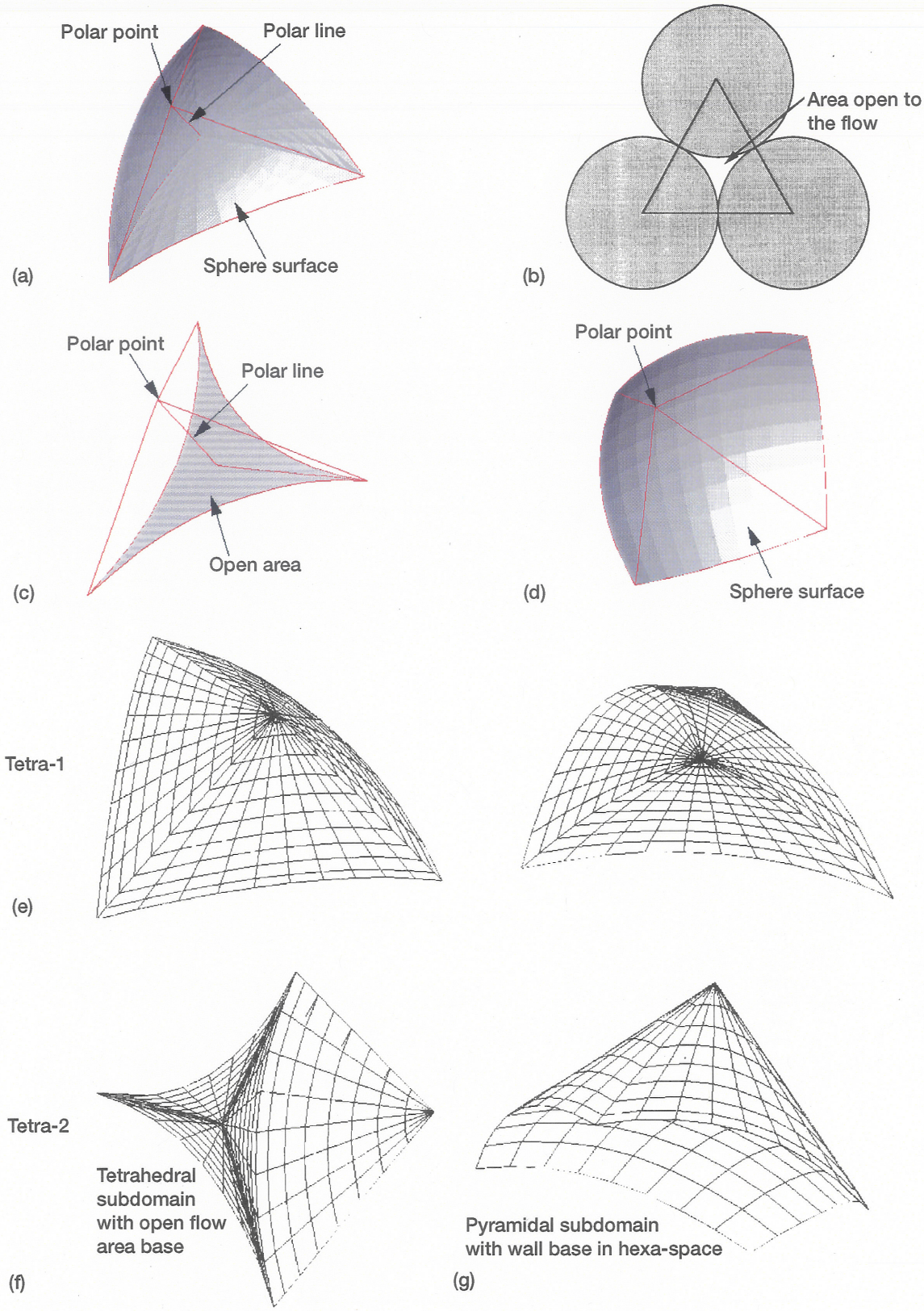

Figure 3.—Outlines of the three basic subdomains used in the tetra- and hexa-spaces. (a) Tetrahedral-1. (b) The cutting plane used to define the outer boundaries of the two clusters. View along the normal to the cutting plane. (c) Tetrahedral-2. (d) Pyramidal. (e) Grid for tetrahedral-1 subdomain with sphere wall base in tetra-space. (f) Grid for tetrahedral-2 subdomains used in the tetra-and hexa-spaces. (g) Grid for pyramidal subdomain used in hexa-space.

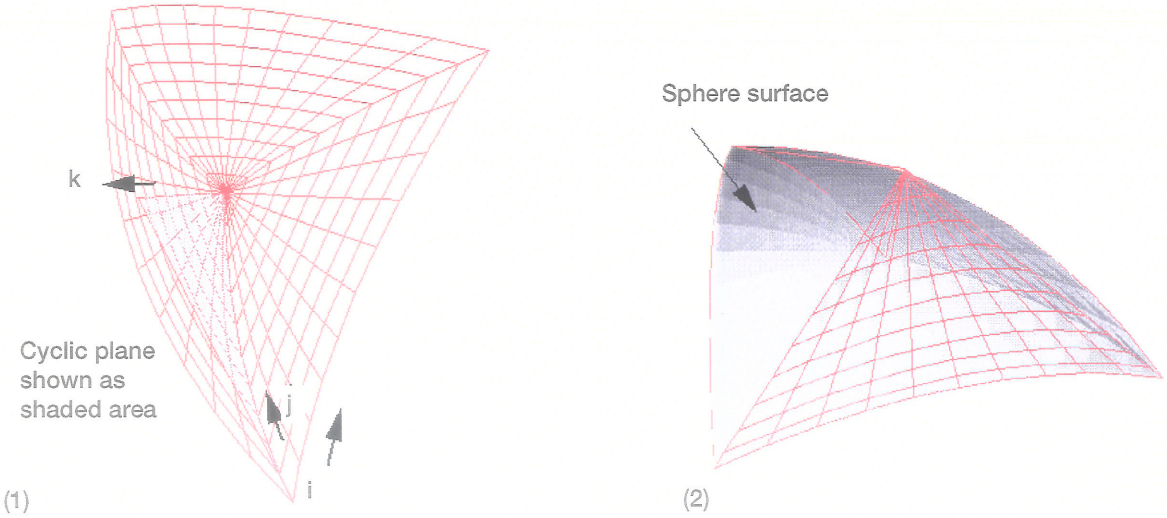

Figure 4(a)—Surface grids for tetrahedral-1 subdomain with axis convention. (1) Grid on the sphere surface. (2) Grid on one of the triangular sides.

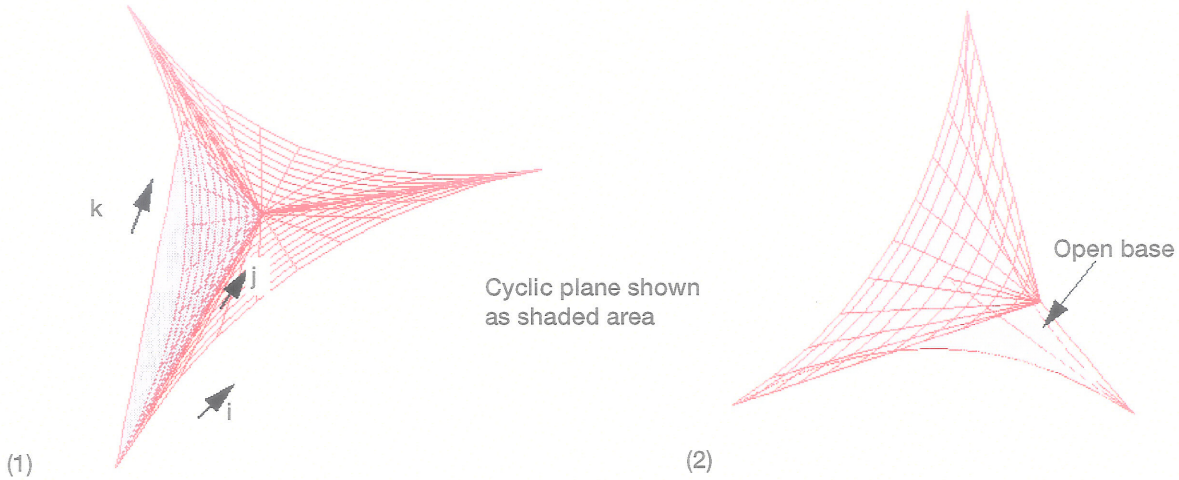

Figure 4(b)—Surface grids for tetrahedral-2 subdomain with axis convention. (1) Grid on the open base area. (2) Grid on one of the triangular sides.

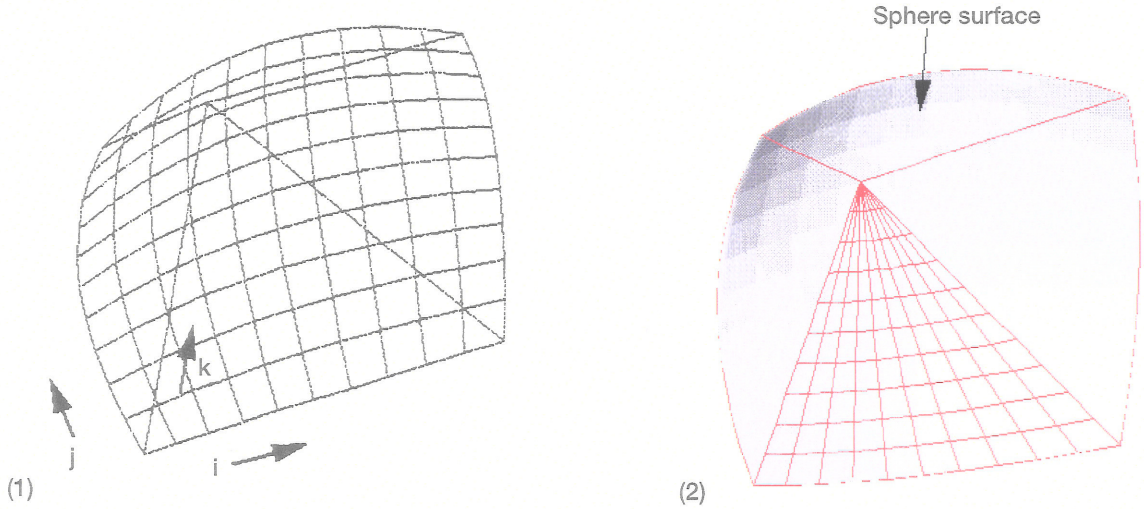

Figure 4(c)—Surface grids for pyramidal subdomain with axis convention. (1) Grid on the sphere surface. (2) Grid on one of the triangular sides.

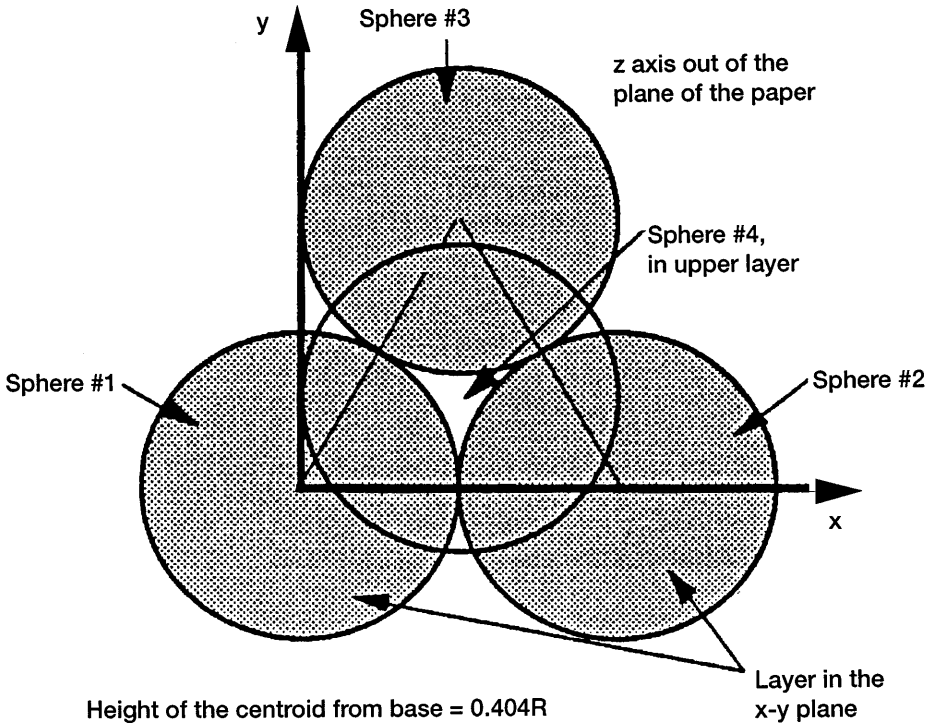

Height of the centroid from base = 0.404R
Height of the center sphere #4 = 1.6329R

(a)

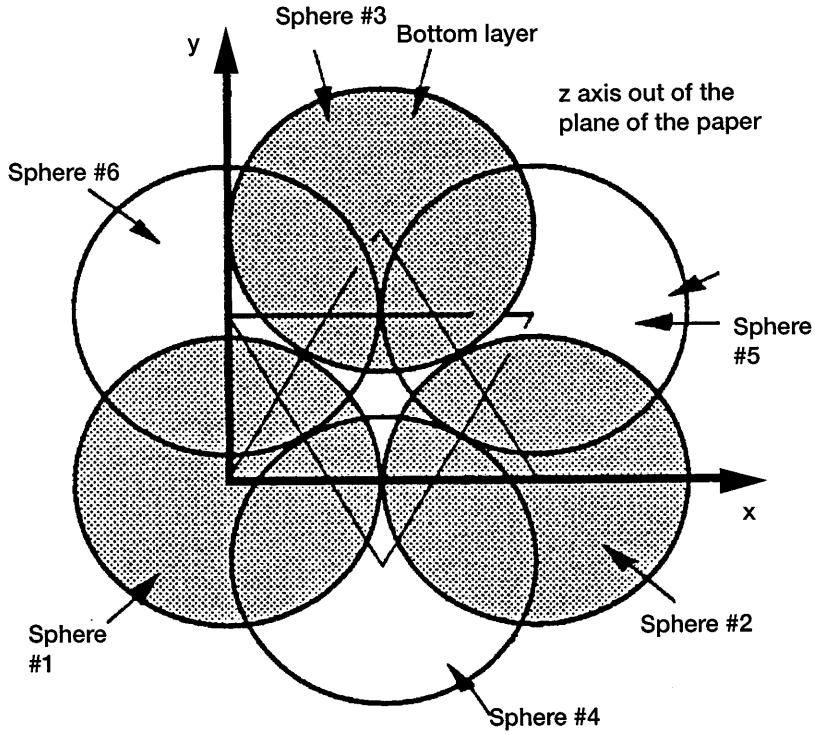

Height of the centroid from base = 0.817R
Height of the sphere centers in upper layer = 1.63299R

(b)

Figure 5.—(a) Axis convention and sphere arrangement for the tetra-space. (b) Axis convention and sphere arrangement for the hexa-space.

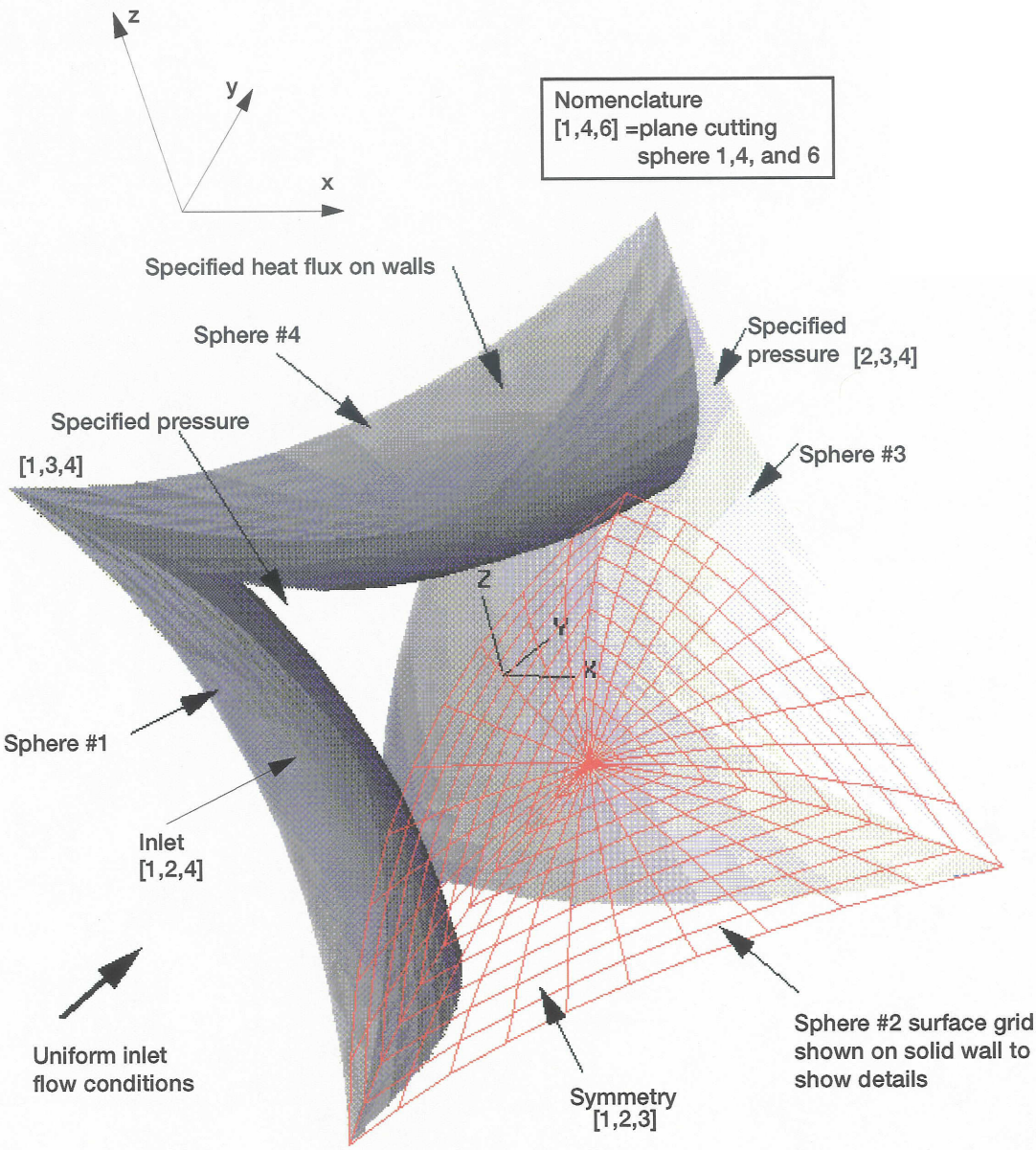

Figure 6(a).—Solids model, flow geometry and boundary conditions for the single tetra-space.

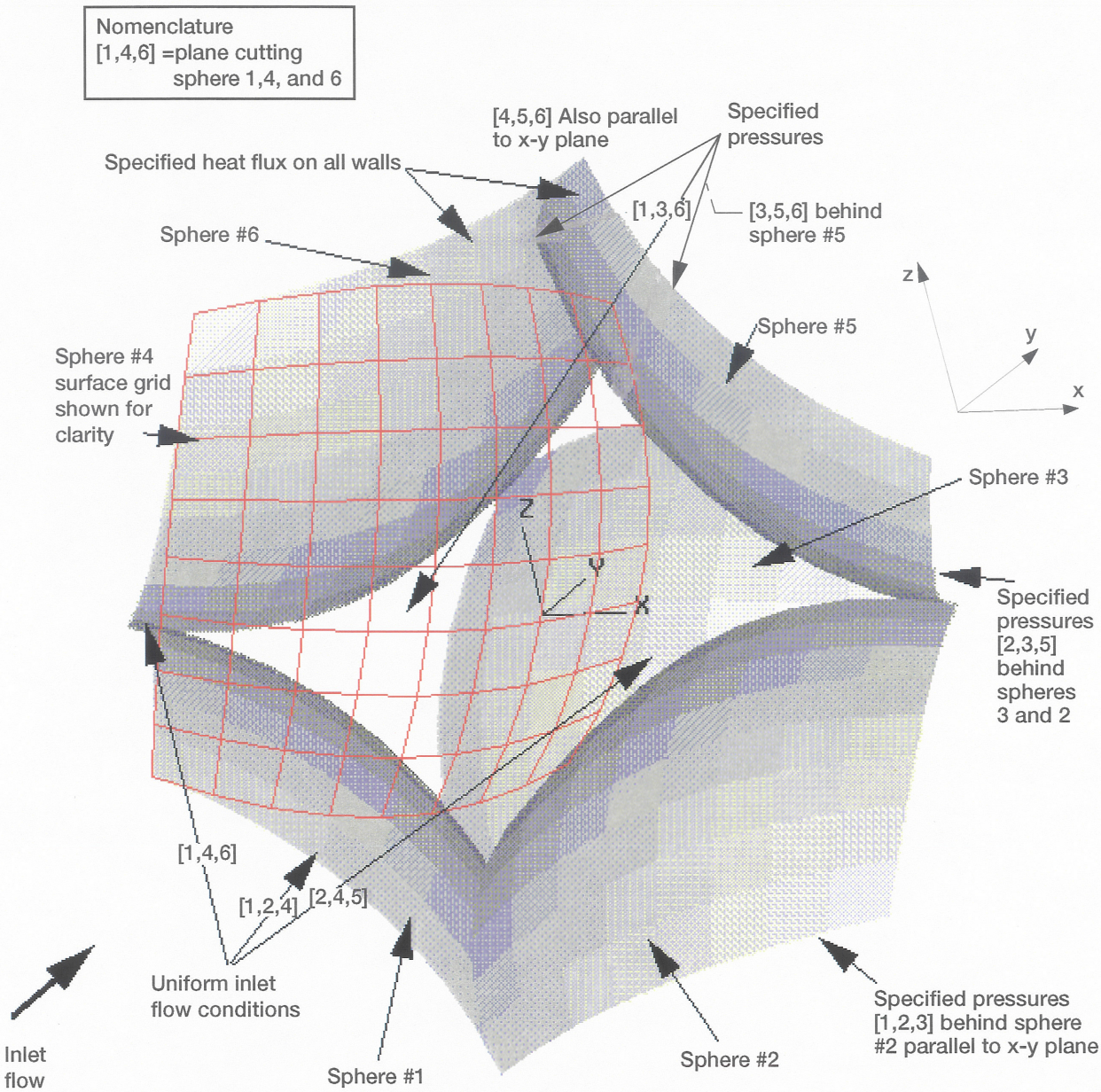

Figure 6(b).—Solids Model, flow geometry and boundary conditions for the single hexa-space.

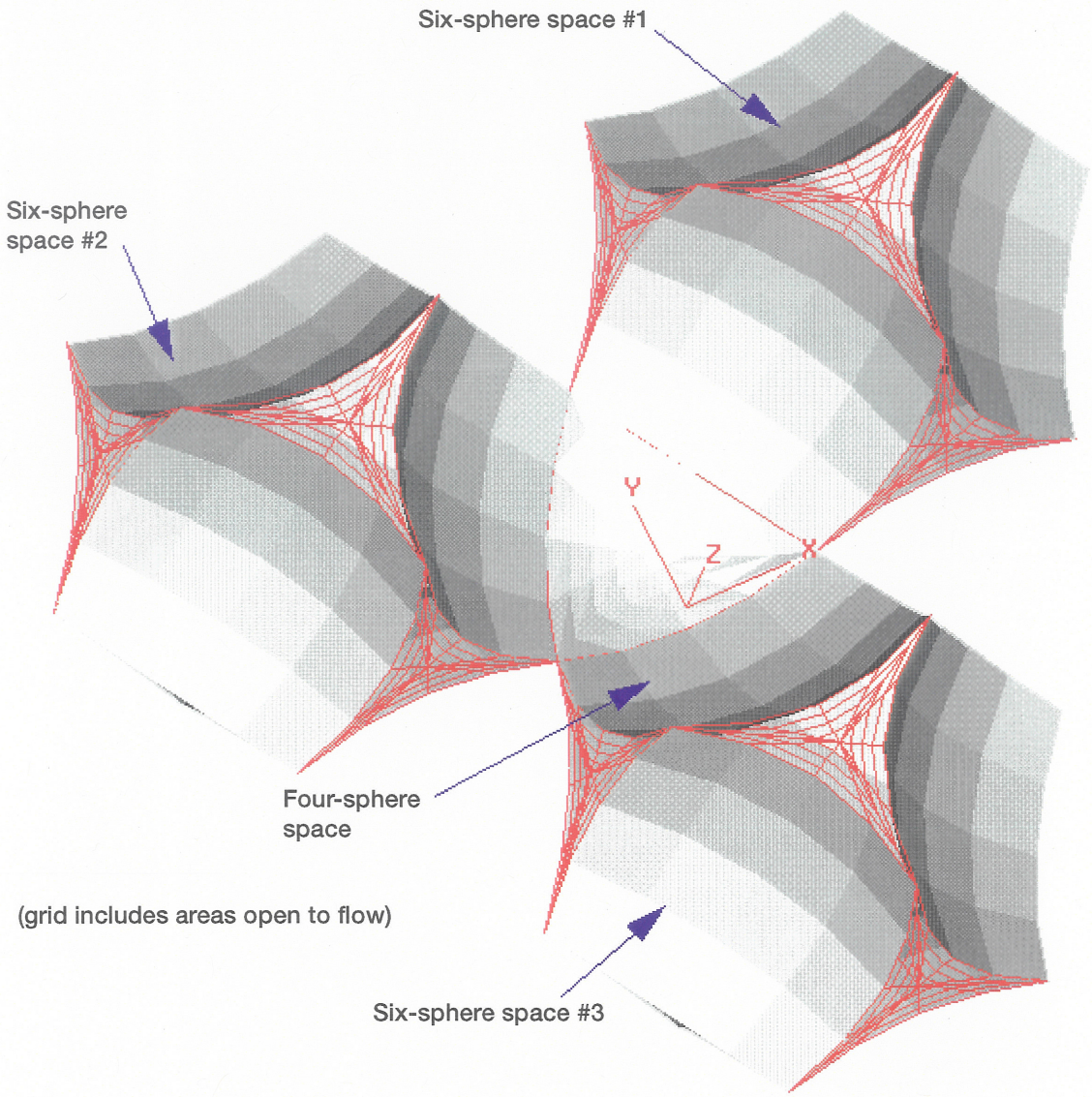

Figure 7(a).—Perspective view of hypercluster-1. Tetra-space in center, three hexa-spaces surrounding it.

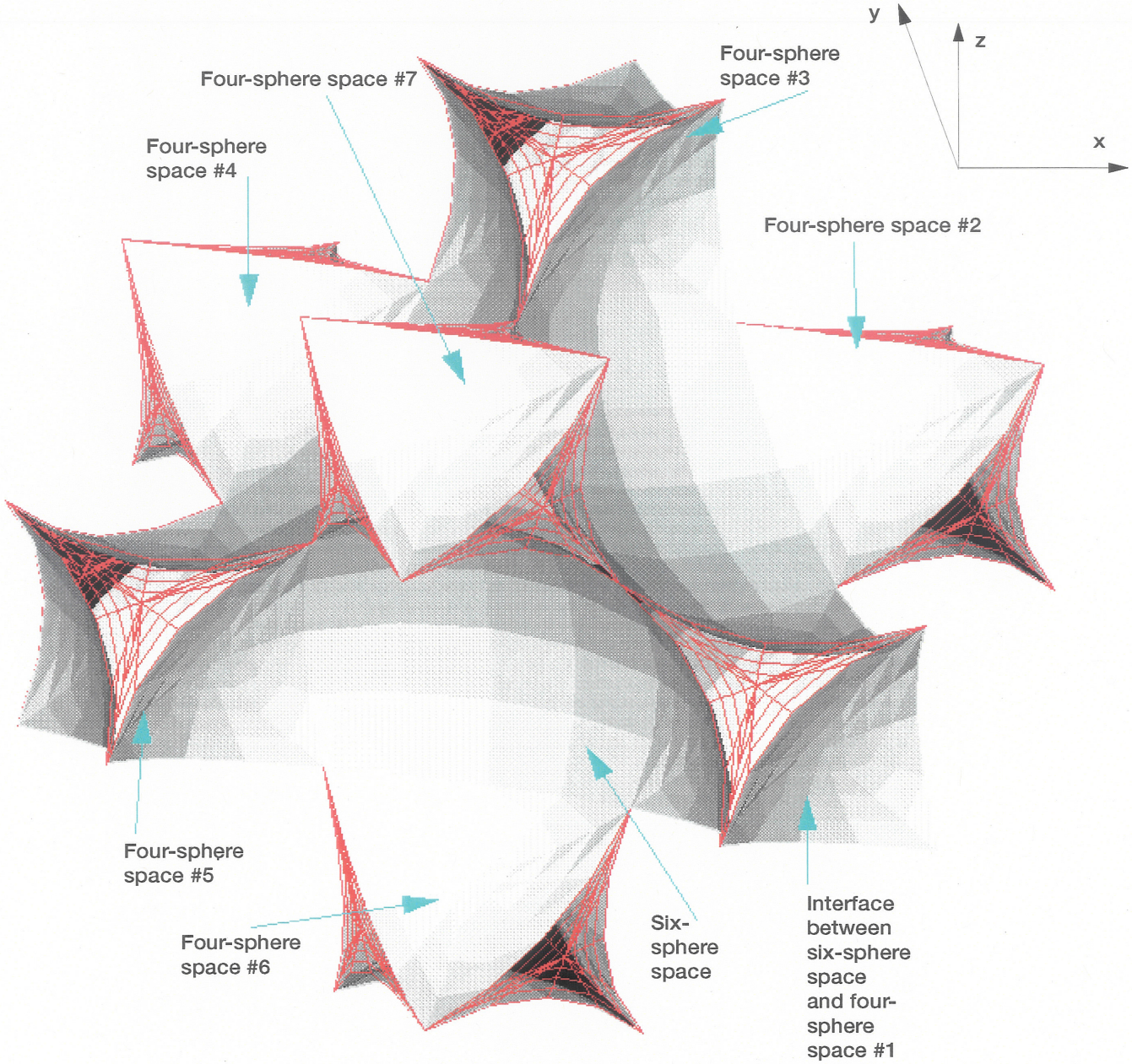

Figure 7(b).—Per-perspective view of hypercluster-2. One hexa-space in center, eight tetra-spaces surrounding it.

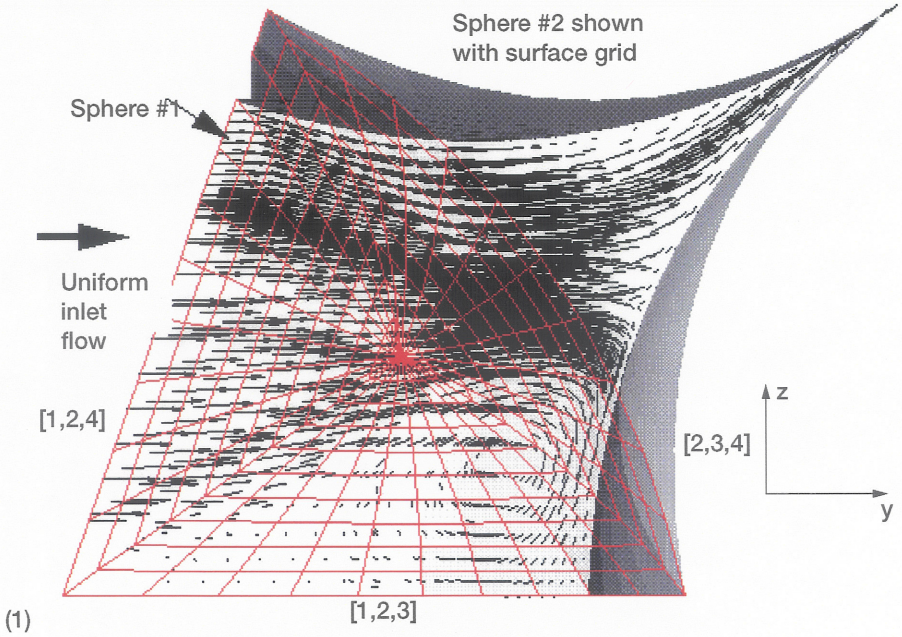

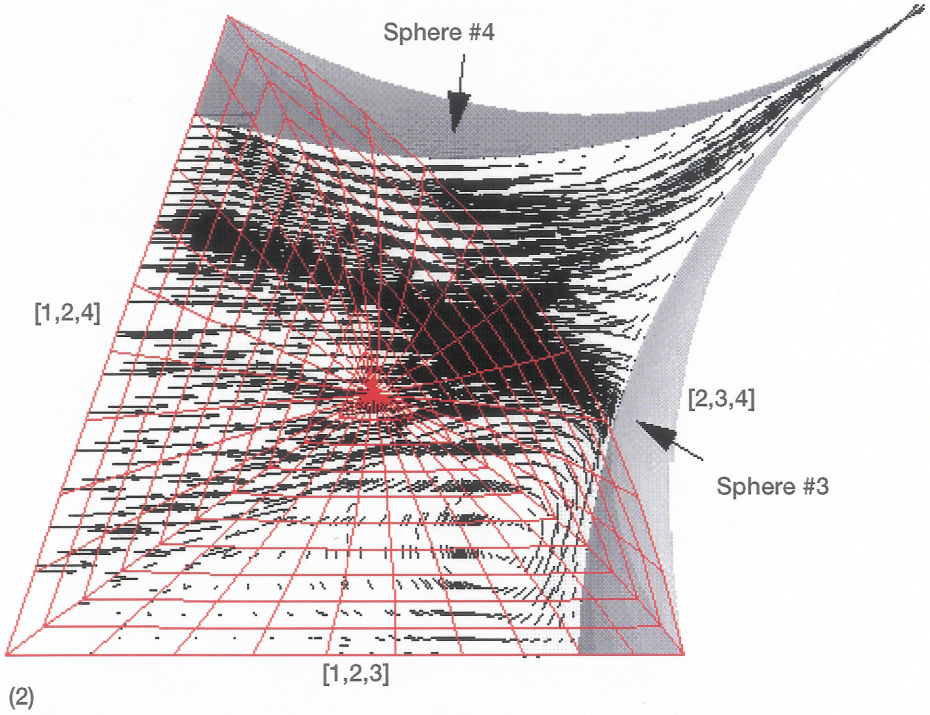

Figure 8(a).—Velocity vectors in the single tetra-space along the x = 1.1 cutting plane. (1) Reynolds number = 400. (2) Reynolds number = 1200.

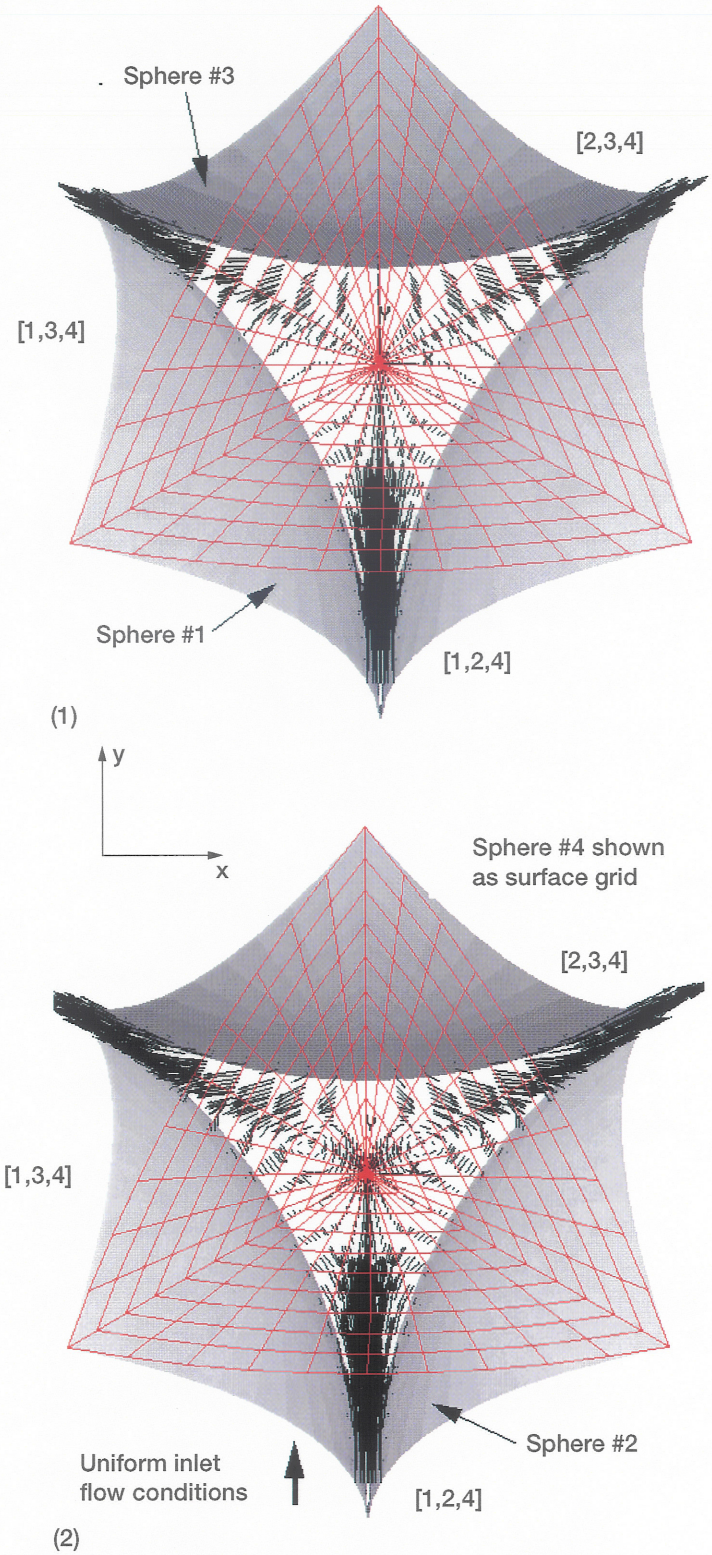

Figure 8(b).—Velocity vectors in the single tetra-space along the z = 0.180 cutting plane. (1) Reynolds number = 400. (2) Reynolds number = 1200.

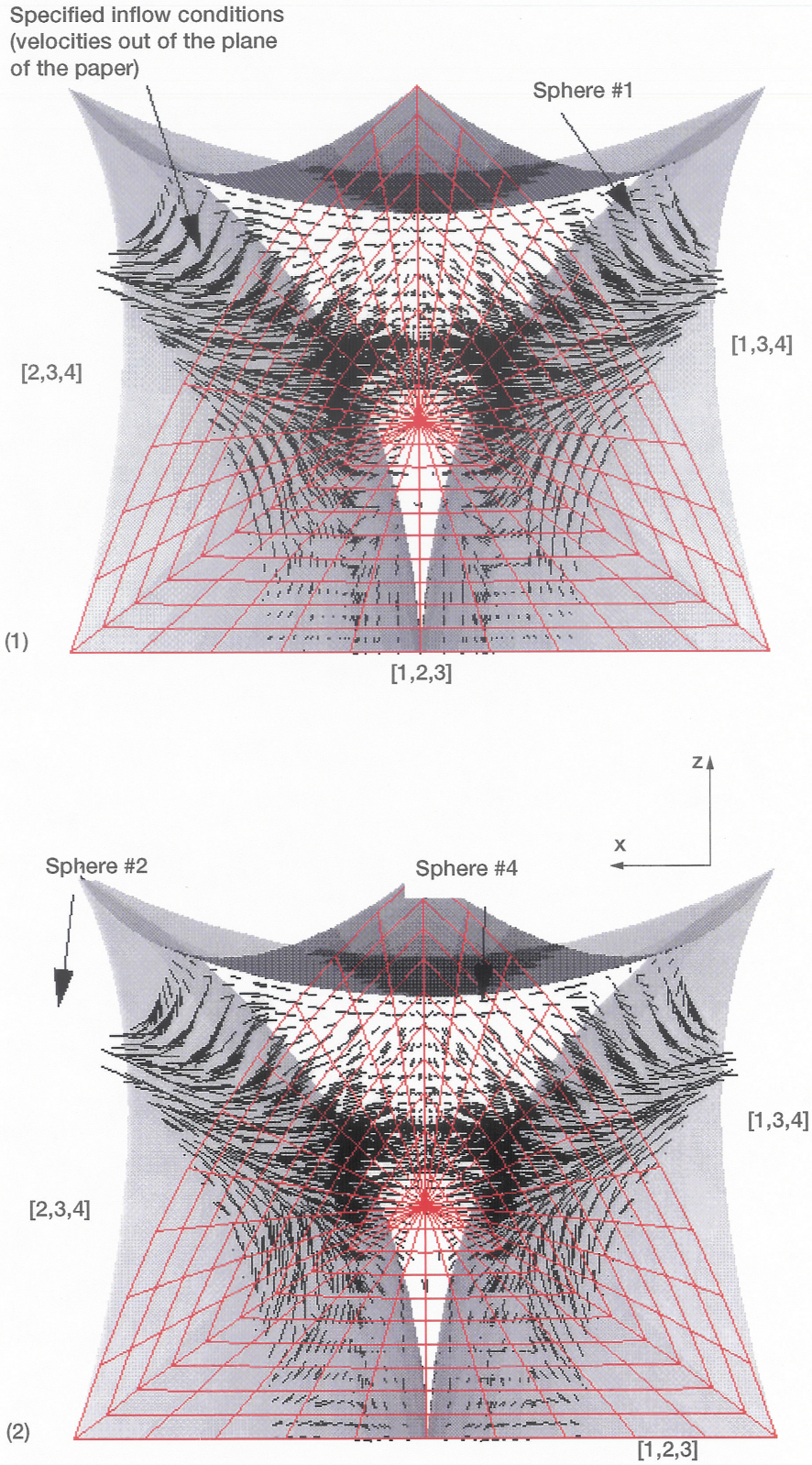

Figure 8(c).—Velocity vectors in the single tetra-space along the y = 0.630 cutting plane. (1) Reynolds number = 400. (2) Reynolds number = 1200.

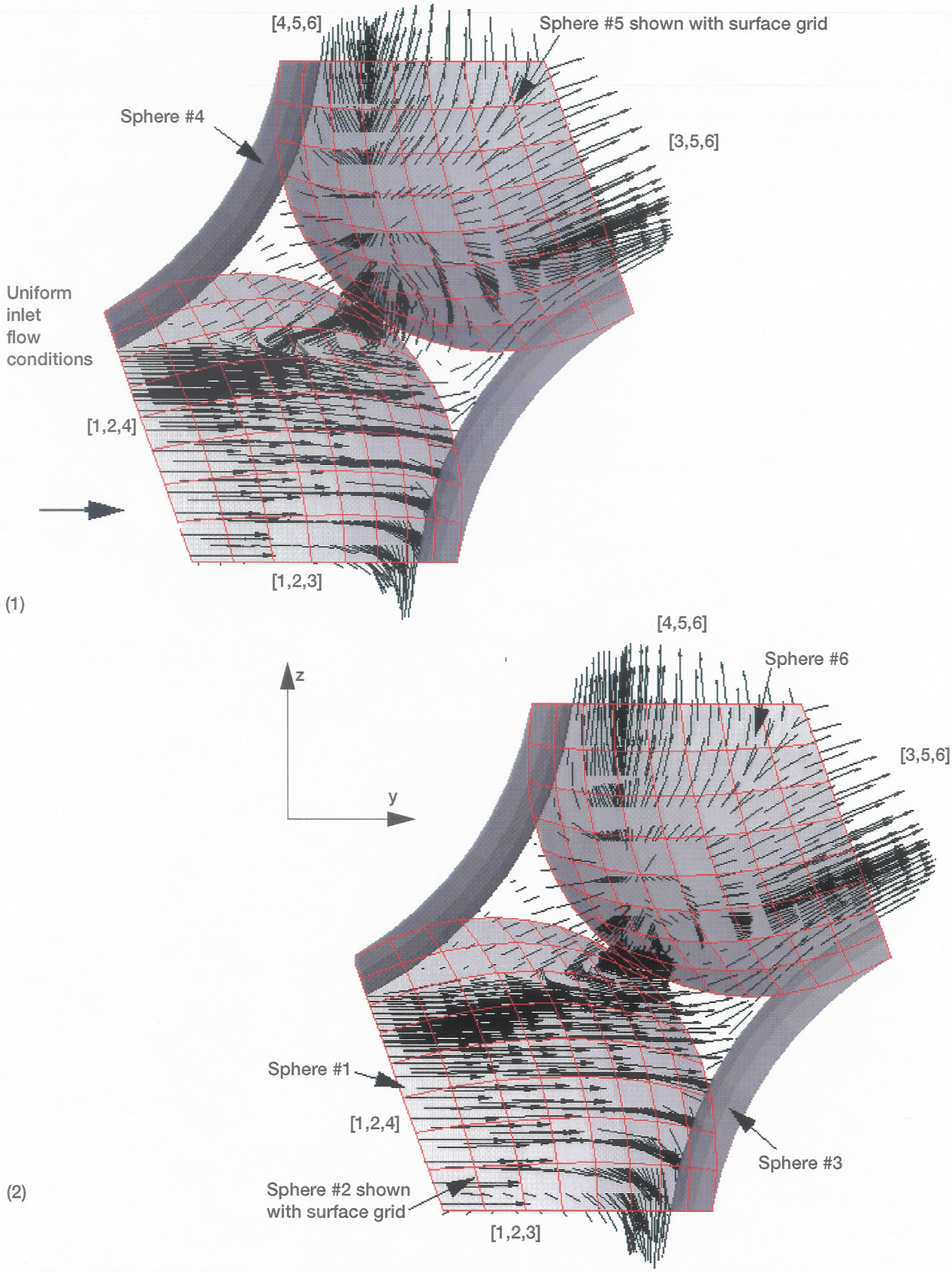

Figure 9(a).—Velocity vectors in the single hexa-space along the x = 1.00 cutting plane. (1) Reynolds number = 400. (2) Reynolds number = 1200.

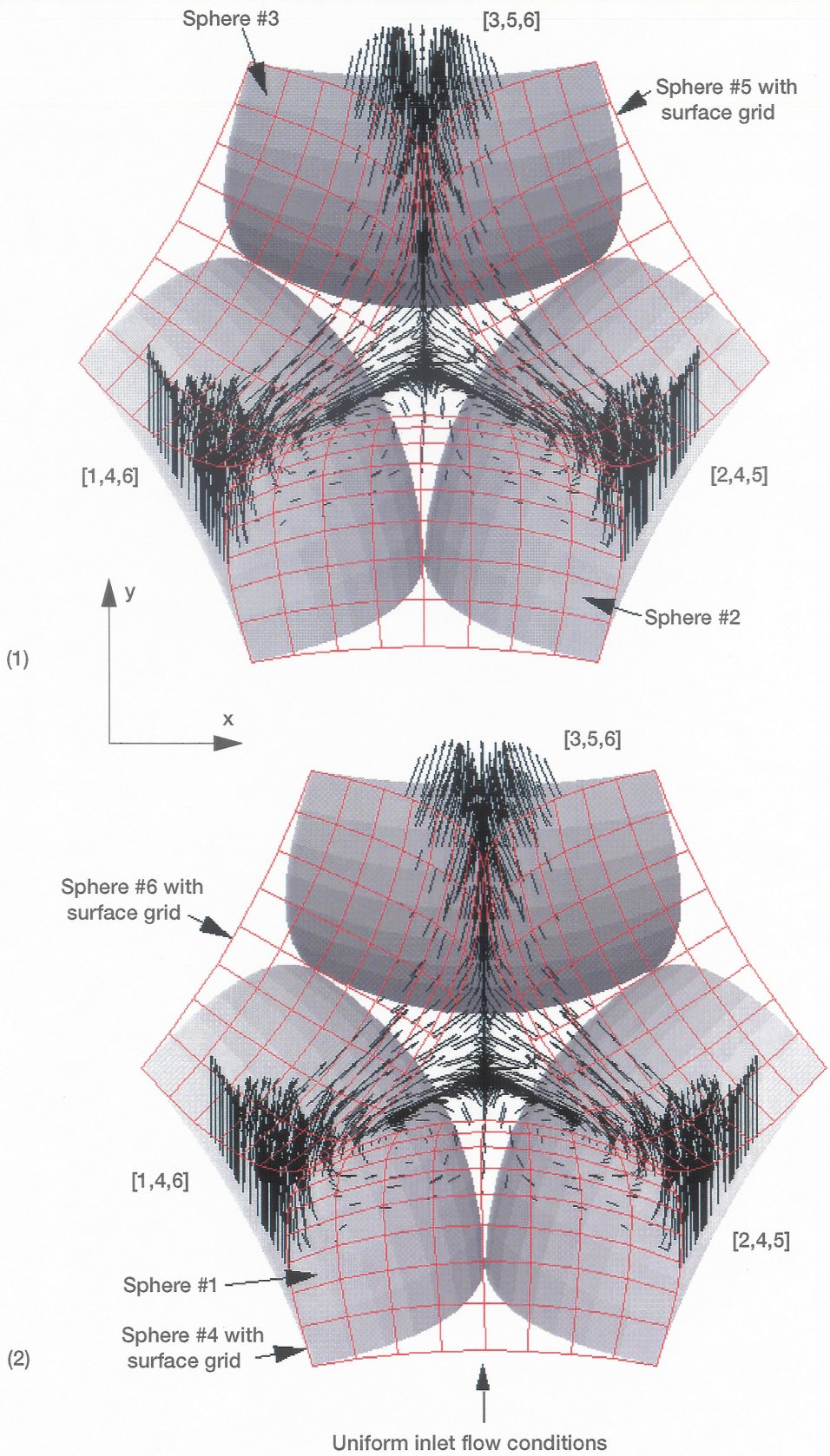

Figure 9(b).—Velocity vectors in the single hexa-space along the z = 1.04 cutting plane. (1) Reynolds number = 400. (2) Reynolds number = 1200.

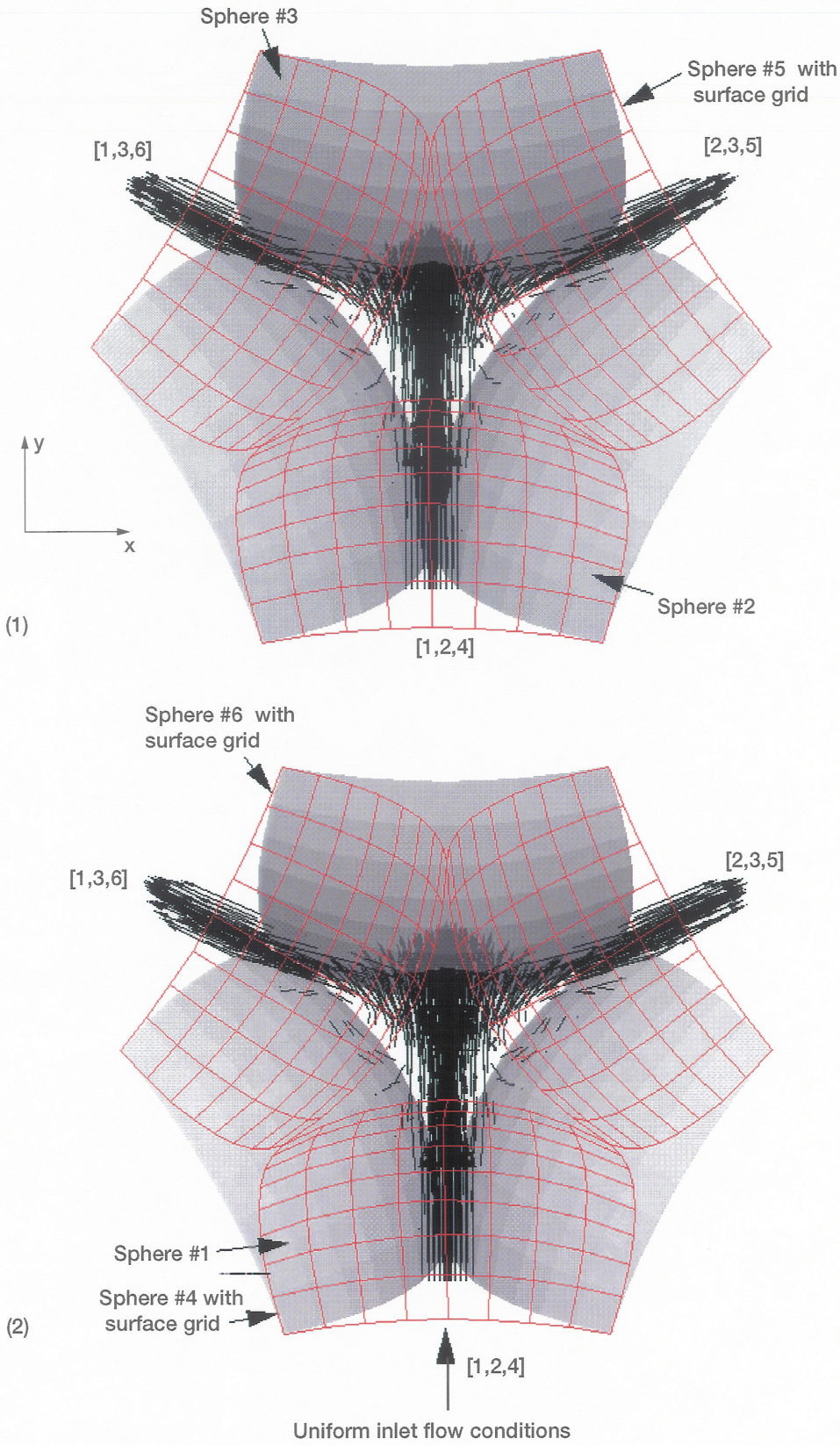

Figure 9(c).—Velocity vectors in the single hexa-space along the z = 0.36 cutting plane. (1) Reynolds number = 400. (2) Reynolds number = 1200.

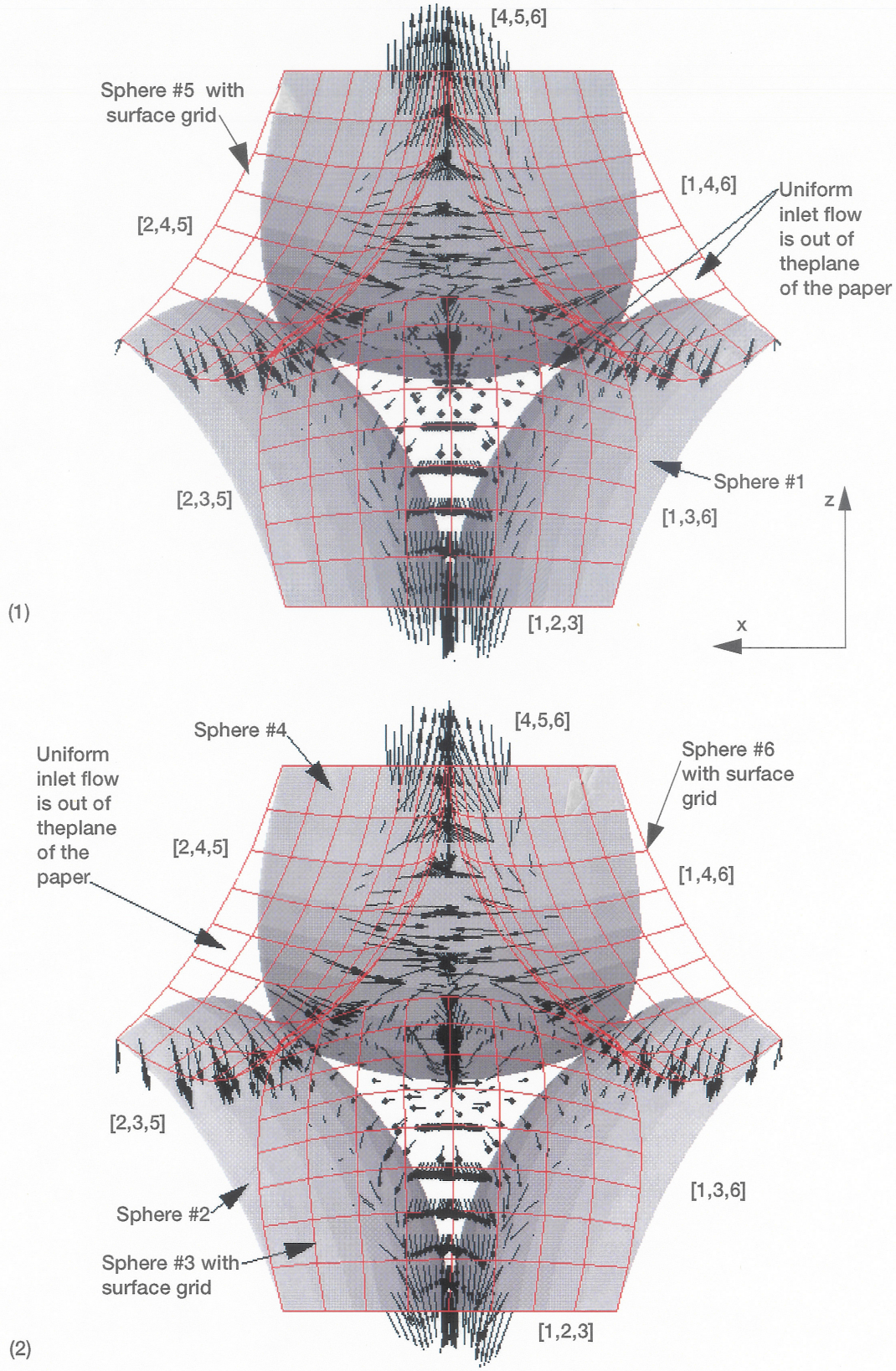

Figure 9(d).—Velocity vectors in the single hexa-space along the y = 0.580 cutting plane. (1) Reynolds number = 400. (2) Reynolds number = 1200.

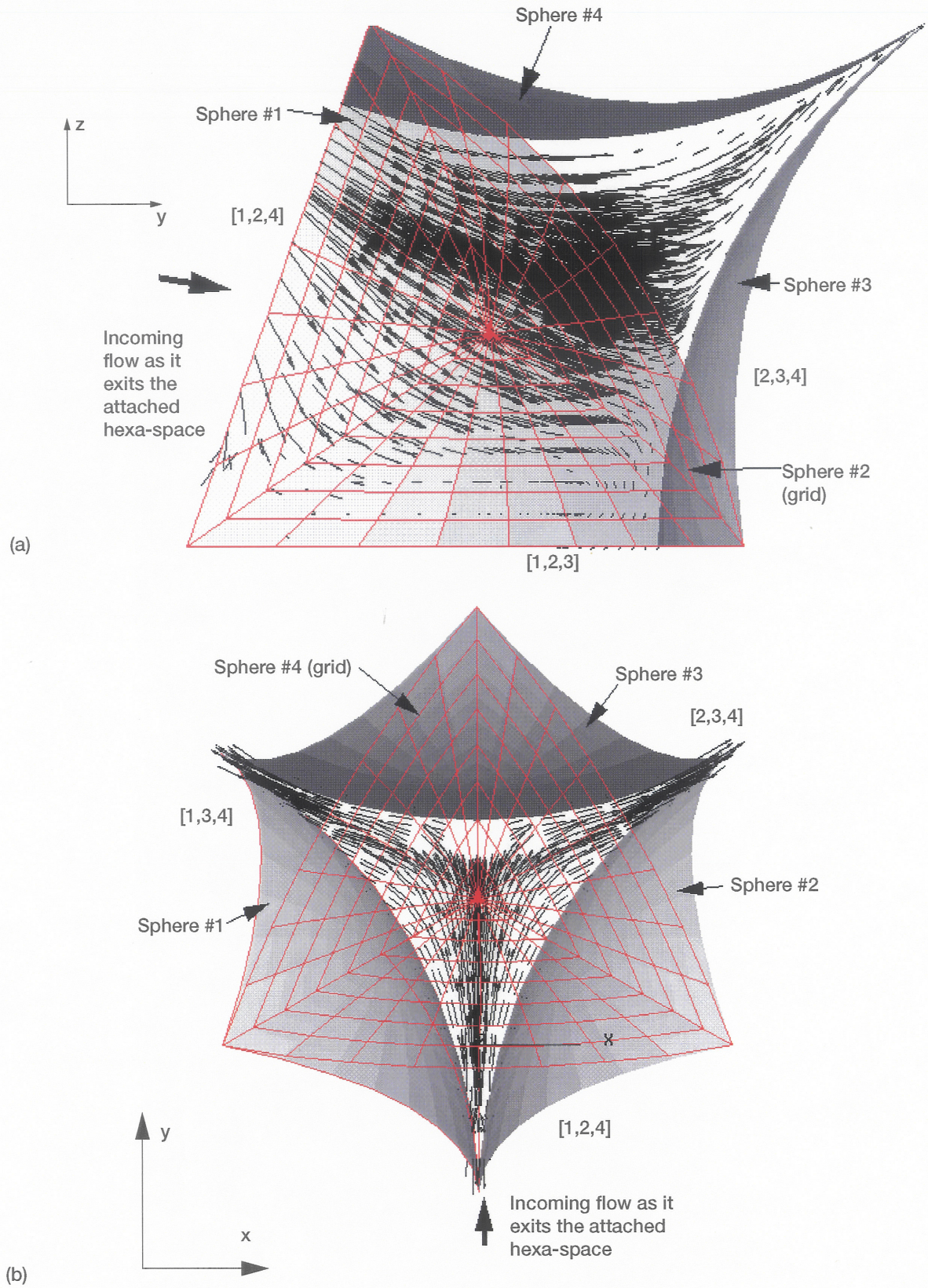

Figure 10.—Hypercluster-1 velocity vectors plots (Reynolds number of 1200). (a) Along x = 1.01 plane (compare fig. 8(a.2)). (b) Along z = 0.180 plane (compare fig. 8(b.2)).

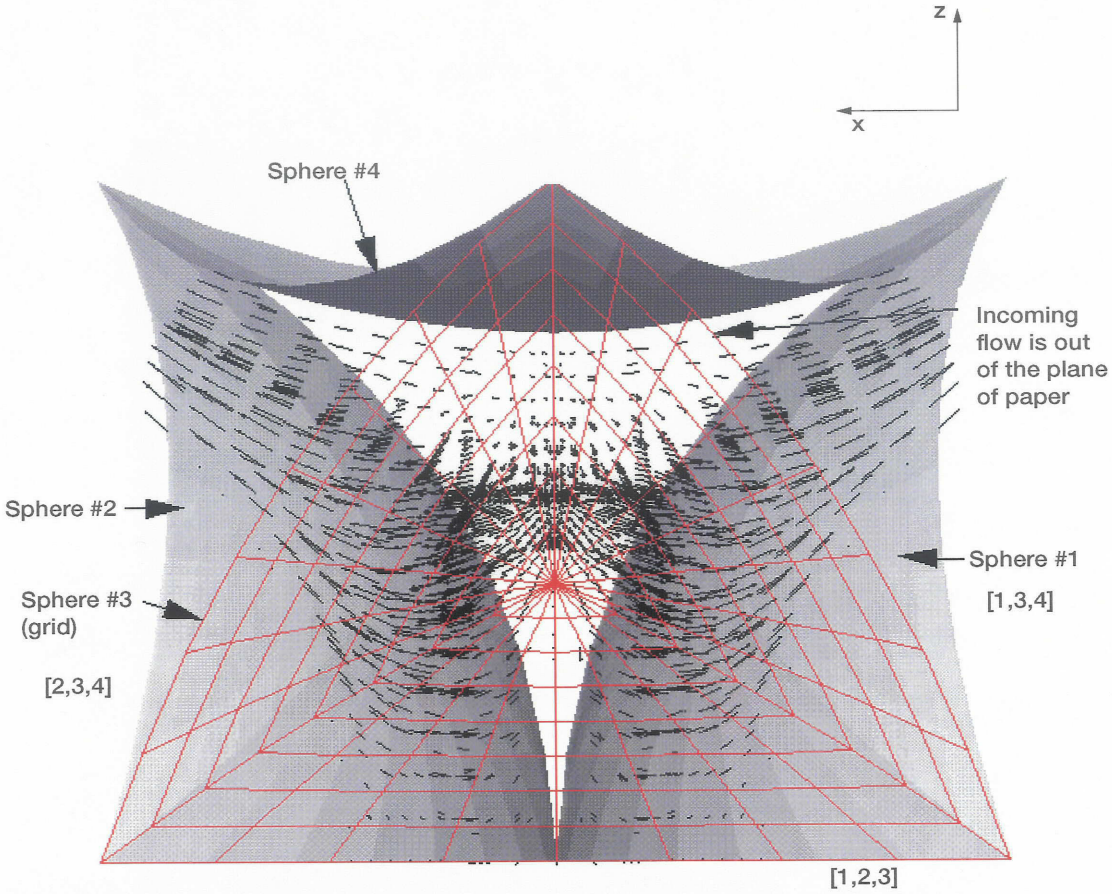

Figure 10(c).—Hypercluster-1 velocity vectors plots (Reynolds number of 1200). (c) Along y = 0.630 cutting plane. Vectors shown only for the central tetra-space (compare fig. 8(c.2)).

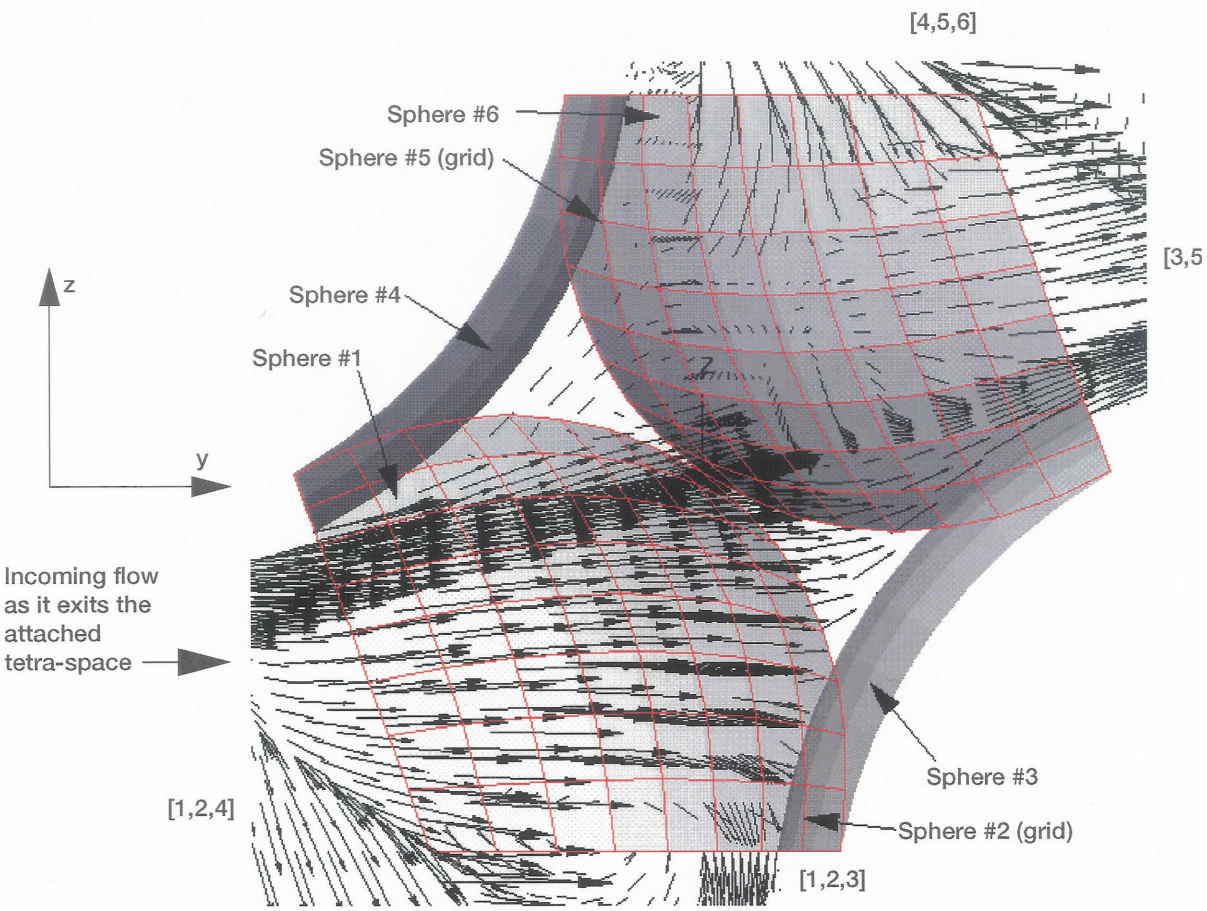

Figure 11(a).—Velocity vector plots for hypercluster-1 (Reynolds number of 1200). Vectors shown only for the central hexa-space. Along x = 1.00 cutting plane (compare fig. 9(a.2))

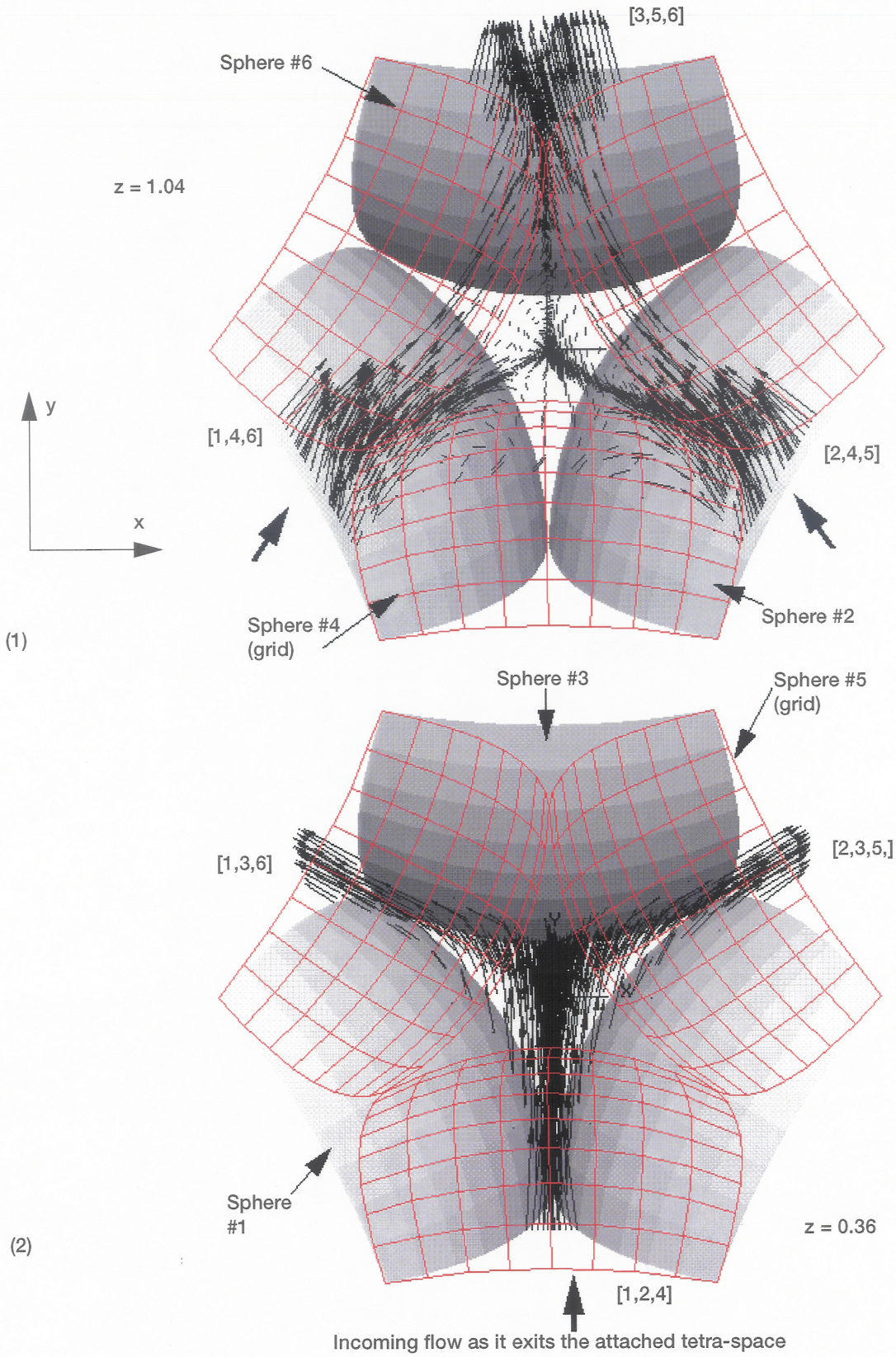

Figure 11(b).—Velocity vector plots for hypercluster-1. Vectors shown only for the central hexa-space. Along z = constant cutting planes. (1) z = 1.04 (compare fig. 9(b.2)); (2) z = 0.36 (compare fig. 9(c.2)).

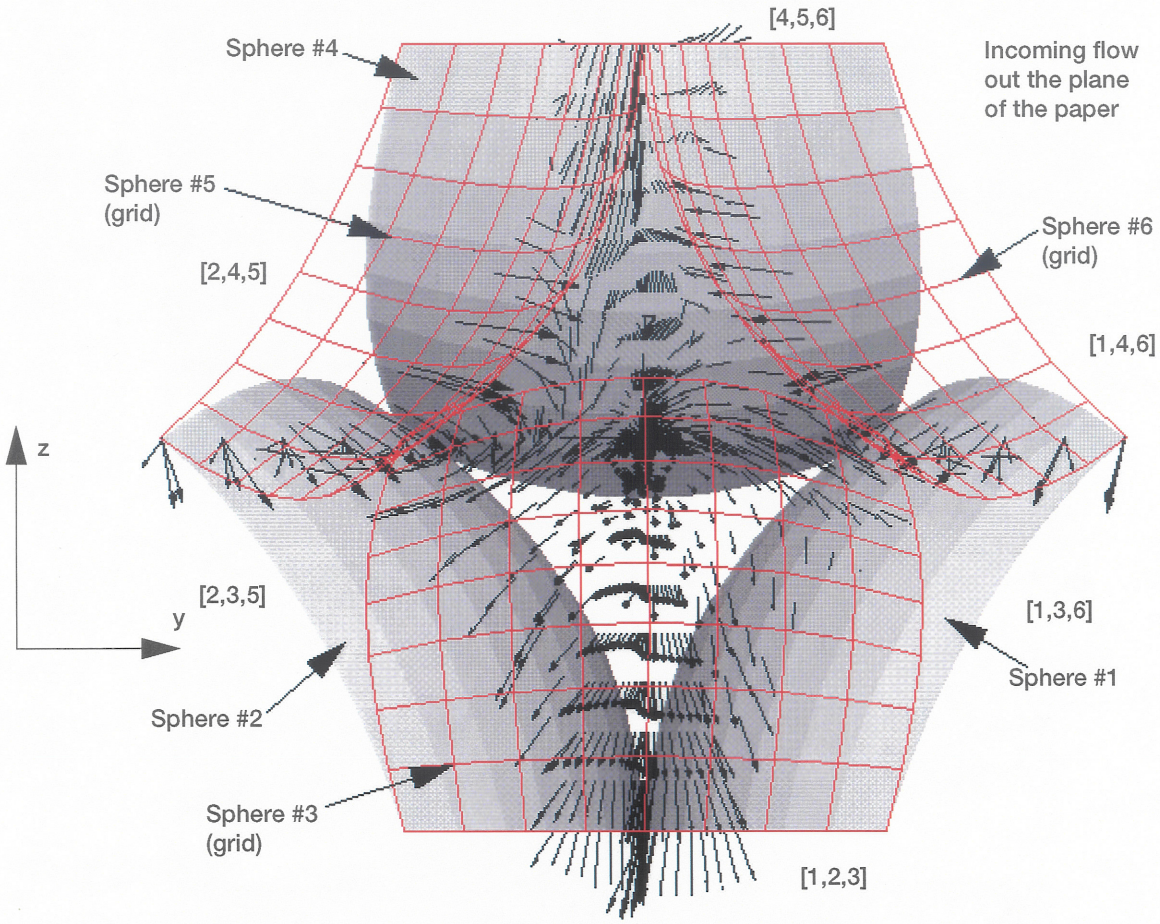

Figure 11(c).—Velocity vector plots for hypercluster-1. Vectors shown only for the central hexa-space. Along y = 0.580 cutting plane (compare fig. 9(d.2)).

REPORT DOCUMENTATION PAGE

Form Approved
OMB No. 0704-0188

Public reporting burden for this collection of information is estimated to average 1 hour per response, including the time for reviewing instructions, searching existing data sources, gathering and maintaining the data needed, and completing and reviewing the collection of information. Send comments regarding this burden estimate or any other aspect of this collection of information, including suggestions for reducing this burden, to Washington Headquarters Services, Directorate for Information Operations and Reports, 1215 Jefferson Davis Highway, Suite 1204, Arlington, VA 22202-4302, and to the Office of Management and Budget, Paperwork Reduction Project (0704-0188), Washington, DC 20503.

1. AGENCY USE ONLY (*Leave blank*)

2. REPORT DATE
February 1997

3. REPORT TYPE AND DATES COVERED
Technical Memorandum

4. TITLE AND SUBTITLE
Numerical Flow Visualization in Basic- and Hyper-Cluster Spheres

5. FUNDING NUMBERS
WU–233–1B–1B

6. AUTHOR(S)
R.C. Hendricks, M.M. Athavale, M.J. Braun, and S. Lattime

7. PERFORMING ORGANIZATION NAME(S) AND ADDRESS(ES)
National Aeronautics and Space Administration
Lewis Research Center
Cleveland, Ohio 44135–3191

8. PERFORMING ORGANIZATION REPORT NUMBER
E–10521-1

9. SPONSORING/MONITORING AGENCY NAME(S) AND ADDRESS(ES)
National Aeronautics and Space Administration
Washington, DC 20546–0001

10. SPONSORING/MONITORING AGENCY REPORT NUMBER
NASA TM–107361

11. SUPPLEMENTARY NOTES
Prepared for the First Pacific Symposium on Flow Visualization and Image Processing sponsored by the Pacific Center of Thermal-Fluids Engineering, Honolulu, Hawaii, February 23–26, 1997. R.C. Hendricks, NASA Lewis Research Center; M.M. Athavale, CFD Research Corporation, Huntsville, Alabama 35805; M.J. Braun, University of Akron, Akron, Ohio 44325; and S. Lattime, B&C Engineering, Akron, Ohio 44325. Responsible person, R.C. Hendricks, organization code 5000, (216) 977–7507.

12a. DISTRIBUTION/AVAILABILITY STATEMENT
Unclassified - Unlimited
Subject Categories 07 and 20

This publication is available from the NASA Center for AeroSpace Information, (301) 621–0390.

12b. DISTRIBUTION CODE

13. ABSTRACT ***(Maximum 200 words)***

Packed spherical particle beds have wide applications throughout the process industry and are usually analyzed using an appropriate combination of laminar and turbulent flows with empirically derived coefficients of which the Ergun (1952) relation is probably the best known. The 3-D complexity of the void distribution within the beds has precluded detailed studies of sphere clusters. Numerical modeling and flow vector visualization for the basic tetra- and hexa-sphere clusters and two hyper-sphere clusters are presented at two Reynolds numbers, 400 and 1200. Cutting planes are used to enable visualization of the complex flows generated within the sphere clusters and are discussed herein. The boundary conditions and flow fields for the simple clusters are also compared to the hyper-clusters with larger variations found for hexa-clusters.

14. SUBJECT TERMS
Porous media; Packed beds; Numerical visualization; CFD; Spheres

15. NUMBER OF PAGES
25

16. PRICE CODE
A03

17. SECURITY CLASSIFICATION OF REPORT
Unclassified

18. SECURITY CLASSIFICATION OF THIS PAGE
Unclassified

19. SECURITY CLASSIFICATION OF ABSTRACT
Unclassified

20. LIMITATION OF ABSTRACT